Available online at www.sciencedirect.com

SciVerse ScienceDirect

Ceramics International 38 (2012) 4771–4782

CERAMICS INTERNATIONAL

www.elsevier.com/locate/ceramint

Effect of La^{3+} substitution on the structural and magnetocrystalline anisotropy of nanocrystalline cobalt ferrite ($CoFe_{2-x}La_xO_4$)

Lawrence Kumar [a,b], Manoranjan Kar [a,*]

[a] Department of Physics, Indian Institute of Technology Patna, Patna 800013, India
[b] Centre for Nanotechnology, Central University of Jharkhand, Ranchi 8352085, India

Received 11 January 2012; received in revised form 21 February 2012; accepted 22 February 2012
Available online 3 March 2012

Abstract

$CoFe_{2-x}La_xO_4$ ($x = 0.0$, 0.025, 0.05, 0.075 and 0.1) samples with different crystallite sizes have been synthesized by the citrate precursor method. All the XRD patterns could be analyzed by the Rietveld refinement technique using the $Fd\bar{3}m$ space group. The cations distribution between the tetrahedral (A-site) and octahedral sites (B-site) has been estimated by Rietveld analysis. The refinement results show that La^{3+} ions have strong preference for octahedral sites (B-sites). The presence of Co, Fe, La and O ions in the sample has been obtained by energy dispersive spectroscopy (EDS) with the help of Field Emission Scanning Electron Microscopy (FE-SEM). The saturation magnetization has been analyzed by the ''Law of Approach (LA)'' technique. The saturation magnetization, magnetic coercivity and magnetocrystalline anisotropy constants are found to decrease with the increase of La^{3+} concentration. The saturation magnetization, coercivity and magnetocrystalline anisotropy constants increase with the increase of crystallite size.

Keywords: B. X-ray methods; C. Magnetic properties; D. Ferrites; D. Spinels

1. Introduction

Ferrimagnetic spinel ferrites are an important class of magnetic ceramics which have a general molecular formula (A^{2+}) $[B_2{}^{3+}]$ $O_4{}^{2-}$, where A^{2+} and B^{3+} are the divalent and trivalent cations and, it crystallize to face-centered cubic lattice with $Fd\bar{3}m$ space group. The unit cell of spinel ferrite crystal structure consists of cubic closed-pack arrangement of oxygen ions with 64 tetrahedral (A-site) and 32 octahedral interstitial sites (B-site). Out of this, 8 of tetrahedral (A-site) and 16 of octahedral (B-site) sites are occupied by the metal cations. Thus the large fraction of empty interstitial sites makes a considerable open crystal structure which leads to migration of cations among interstitial sites during preparation. The magnetic properties in these ferrites depend on several factors such as, method of preparation, chemical compositions, annealing temperature and distribution of cations among the tetrahedral (A) and octahedral (B) sites [1]. Among the various ferrite materials, cobalt ferrite ($CoFe_2O_4$) has drawn considerable attention due to remarkable properties, such as high coercivity, moderate saturation magnetization along with good mechanical hardness and chemical stability [2]. It is a hard ferrimagnetic material with a high magnetic ordering temperature (around ~520 °C) and it crystallizes in mixed spinel structure with the space group $Fd\bar{3}m$. The mixed spinel structure of cobalt ferrite is represented as $(Co_x{}^{2+}Fe_{1-x}{}^{3+})[Co_{1-x}{}^{2+}Fe_{1+x}{}^{3+}]O_4$, where cations inside the round and square brackets occupy A and B-sites respectively, and x depends on the thermal history and preparation conditions [3]. These cobalt ferrite materials are well known to exhibit large magnetocrystalline anisotropy energy with positive anisotropy constant (K_1) which is a typical feature of the hard magnetic materials [4–6]. This magnetocrystalline anisotropy constant strongly depends upon the synthesis method as well as annealing temperature [7]. For instance, the magnetocrystalline anisotropy constant (K_1) of cobalt ferrite of crystallite size about 35 and 42 nm at room temperature are found to be 2.27×10^6 and 3.90×10^6 erg/cm^3 respectively [7,8]. This material is a versatile magnetic material for technological applications such as, magnetic resonance imaging contrast

* Corresponding author. Tel.: +91 6122552013; fax: +91 6122277383.
E-mail address: mano@iitp.ac.in (M. Kar).

0272-8842/$36.00
doi:10.1016/j.ceramint.2012.02.065

agents, data storage devices, transformer cores, ferrofluid technology, and magneto caloric refrigeration [9–11]. The spinel cobalt ferrite material is a tunable magnetic system. Its magnetic properties can be tuned by replacing A and/or B site with different transition and non transition elements. The recent investigations on the substitutions at the Fe sites of $CoFe_2O_4$ by various cations like Ga, Mn, Al, and Cr have revealed the change in atomic level magnetic interactions and, have induced different magnetic properties [12–15]. Magnetic properties can be promisingly modified for cobalt ferrites by doping the rare earth elements. The carriers of magnetism in rare earth elements are the 4f electrons. The RE^{3+} ions possess a wide variety of magnetic properties as their magnetic moments vary from 0 (La^{3+}) to 10.5 μ_B (Dy^{3+}) [16–20]. The magnetic properties in spinel cobalt ferrite are mainly due to a predominant superexchange interaction between the cations in the A-site and B-site via oxygen ions, i.e. the magnetic behavior is largely governed by the spin coupling of the 3d electrons [21]. One can expect an appearance of spin coupling of 3d-4f electrons by substitution of small amount of rare earth cations (RE^{3+}, i.e. the 4f elements series) in place of Fe ions. Hence the magnetic properties (change of magnetic moment, magnetocrystalline anisotropy constant, magnetic coercivity, etc.) can be modified. However, the preparation of nanocrystalline rare earth doped cobalt ferrite materials in single phase form suffers from many difficulties. Several authors have reported the synthesis of RE^{3+} substituted nanocrystalline spinel ferrites by the solid state route. It suffers from drawbacks like phase segregation of orthoferrites ($REFeO_3$) [22–26], hematite (α-Fe_2O_3) [27,28] and metal monoxides [29] even for very low RE^{3+} concentration.

There are a few reports available which have mentioned the synthesis of RE^{3+} substituted nanocrystalline spinel ferrites in single phase form using different chemical routes despite having big difference in ionic radius of RE^{3+} and Fe^{3+} ions [16,17,20,30,31]. Substitution of non-magnetic element (Al) in place of Fe ion in $CoFeO_4$ leaves this material with magnetic defect without lattice distortion as ionic size of Al is comparable to that of Fe ions [15]. It does not take part in the exchange interaction to the nearest neighboring ions due to its non-magnetic nature which leads to the weakening of the tetrahedral–octahedral superexchange interaction. Hence, the magnetic properties can controlled without complicacy. Similarly La^{3+} is non-magnetic rare earth cation as it has no 4f electrons [2]. However, its ionic size is much larger than the ionic size of Fe and Co ions. So, little amount solid solution of La^{3+} in $CoFe_2O_4$ may create lattice strain in the material and it leads to modify the magnetic structure. The magnetic properties can be modified due to change in magnetic structure. In other way, it will not take part in the superexchange interaction and hence avoid the complications. Also another problem in cobalt ferrite to control the crystal size because nucleation rate is very high which restrict to prepare a particular size material to use in technology such as, soft magnetic applications, hyperthermia applications etc. Hence, by substituting larger ion restrict nucleation due to lattice strain and, hence one can easily prepare desired size materials for technological applications. Also La^{3+} exhibits only in 3+ state which restrict it to enter into B-site only. Above discussion reveals that, La^{3+} substitution in place of Fe in cobalt ferrite has advantage over the transition element substitutions in place of Fe in $CoFe_2O_4$. Hence our aim is to tune the physical properties of cobalt ferrite by substituting non-magnetic La^{3+} in place of Fe ions in $CoFe_2O_4$. These materials can be used for soft magnetic applications such as memory devices and hyperthermia applications. Also the substitution of La^{3+} cation in place of Fe in $CoFe_2O_4$ are promising for their magneto optical recording applications as they would be helpful in reducing the curie temperature compared to pure ferrite. The incorporation of La^{3+} ions results in increase in dc resistivity which makes the materials suitable for the high frequency applications where eddy current loss becomes appreciable.

The structural and magnetic properties of La^{3+} substituted nanocrystalline cobalt ferrite have been reported by various groups. Kumar et al. [32] have synthesized La^{3+} substituted cobalt ferrite nanocrystalline materials ($CoFe_{2-x}La_xO_4$, $x = 0.0$, 0.1, 0.15, 0.2) using the co-precipitation technique. They have observed that the saturation magnetization decrease with the increase in La^{3+} ions concentration. Kim et al. [30] have synthesized nanocrystalline $CoFe_{1.9}La_{0.1}O_4$ by the sol gel method and observed that, coercivity decreases and saturation magnetization increases with the increase in annealing temperature. Tahar et al. [31] have prepared $CoFe_{1.9}La_{0.1}O_4$ nanoparticles by the polyol method and reported the superparamagnetic of the particles at room temperature. Burianova et al. [33] have synthesized La-doped $CoFe_2O_4$ nanoparticles by microemulsion route and reported that, coercivity values depend on particle size rather than La^{3+} concentration. According to our knowledge, there is lack of detailed study on crystal structure and magnetocrystalline anisotropy of nanocrystalline La^{3+} substituted cobalt ferrite. Hence in this report we have reported the crystal structure and magnetocrystalline anisotropy constant at room temperature of nanocrystalline $CoFe_{2-x}La_xO_4$ ($x = 0.0$, 0.025, 0.05, 0.075 and 0.1) samples.

2. Experimental

Nanocrystalline powders of $CoFe_{2-x}La_xO_4$ for $x = 0.0$, 0.025, 0.05, 0.075 and 0.1 were synthesized by the citrate precursor method. Cobalt nitrate (Co $(NO_3)_2{\cdot}6H_2O$), iron nitrate (Fe $(NO_3)_3{\cdot}9H_2O$), lanthanum oxide (La_2O_3) and citric acid ($C_6H_8O_7{\cdot}H_2O$) with 99.9% purity were used as starting materials. The molar ratio of metal nitrates to citric acid was taken as 1:3. The metal nitrates were dissolved in a deionized water (milli Q grade) to get a solution. An aqueous solution of citric acid was mixed with metal nitrate solutions. The mixed solution was heated at 80 °C with constant stirring using hot plate. The solution became viscous and finally forming brown gel. The gel was dried overnight using an oven at 80 °C in order to remove excess water. During the process of drying, the gel swells into the fluffy mass and eventually broke into brittle flakes. The resulting materials were heat treated in air atmosphere at 200 °C, 600 °C and 800 °C for 2 h at each

temperature. The crystalline phase of the annealed samples was identified by the powder X-ray diffraction method (Rigaku Miniflex) using Cu K_α radiation. The Fourier Transform Infrared Spectra (FT-IR) was recorded with a Perkin Elmer (Model Spectrum 400) within the wave number range of 390–750 cm^{-1}. The compositions of all the samples were studied by EDS (energy-dispersive spectroscopy) using the Hitachi S4800 Field Emission Scanning Electron Microscopy (FE-SEM). The magnetic hysteresis loops were recorded at room temperature by using the LakeShore (Model No. 7410) Vibrating Sample Magnetometer (VSM). The maximum field was used ±1.5 T.

3. Results and discussions

3.1. Structural analysis

XRD patterns of $CoFe_{2-x}La_xO_4$ with $x = 0.0$, 0.025, 0.05, 0.075 and 0.1 are shown in Figs. 1–3 for the samples annealed at 200 °C, 600 °C and 800 °C respectively. All the samples are essentially in single phase form. We have not observed any trace of impurity peaks which confirms that, La^{3+} ions have been incorporated into the spinel lattice. All the XRD peaks could be indexed to $Fd\bar{3}m$ space group in cubic symmetry. The XRD patterns annealed at 200 °C show broader peaks and incomplete crystallization compare to that of annealed at 600 °C and 800 °C. It reveals that thermal energy for 200 °C annealed samples is not sufficient for the incorporation of the La^{3+} ions into the spinel lattice due to large difference in ionic radius of La^{3+} (1.03 Å) and Fe^{3+} (0.64 Å) cations. Therefore, more energy is needed to make La^{3+} ions enter into the spinel lattice to complete the crystallization. The XRD patterns of the samples annealed at 600 °C show an improvement in the sharpness of the peaks and reduction in the peak broadening. The XRD patterns of the samples annealed at 800 °C show that samples are well crystallized into the spinel phase compare to that of annealed at 600 °C. Crystallization of the samples become more difficult and some sort of amorphous-like phases

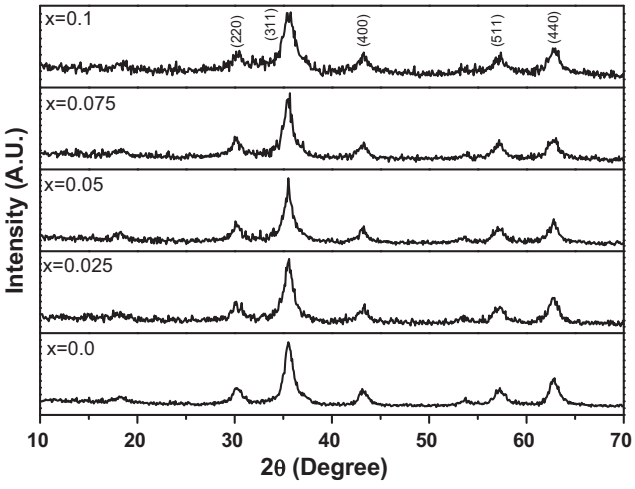

Fig. 1. XRD patterns of the sample $CoFe_{2-x}La_xO_4$ for $x = 0.0$, 0.025, 0.05, 0.075 and 0.1 annealed at 200 °C.

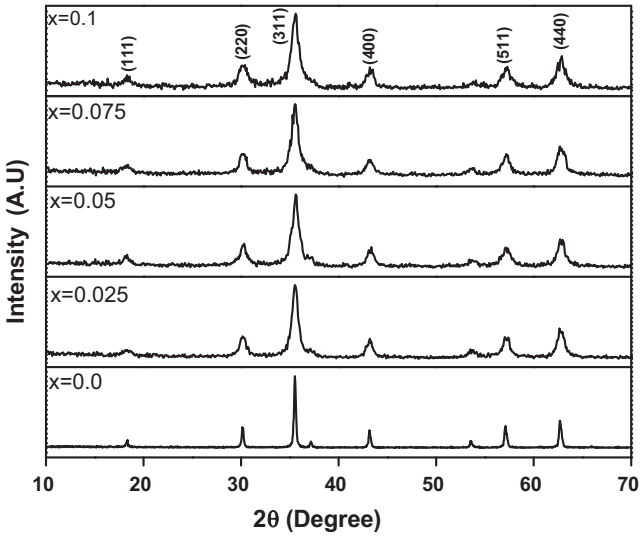

Fig. 2. XRD patterns of the sample $CoFe_{2-x}La_xO_4$ for $x = 0.0$, 0.025, 0.05, 0.075 and 0.1 annealed at 600 °C.

(figure not shown) appear with the gradual increase in La^{3+} concentration. More dopant concentration leads to a higher potential barrier for La^{3+} ion to overcome for entering into the spinel crystal lattice. The samples were annealed at higher temperature (1050 °C) to increase the crystallite size of La^{3+} doped samples. However, we have observed that another phase has segregated as $LaFeO_3$ (figure not shown) in addition to spinel phase. So we conclude that the RE^{3+} ions can be substituted for Fe^{3+} ions only when the samples are in nanocrystalline form. The materials in the nanocrystalline form have a large surface to volume atoms which leads to incorporate larger ions (La^{3+}) compare to Fe^{3+} ions in the lattice sites. It happens because the surface atoms of nanocrystalline materials have less stability in the crystal unit cell. Whereas in the bulk materials, there is high stability of the lattice sites which prevents to incorporate larger ions (La^{3+}) compare to Fe^{3+} ions.

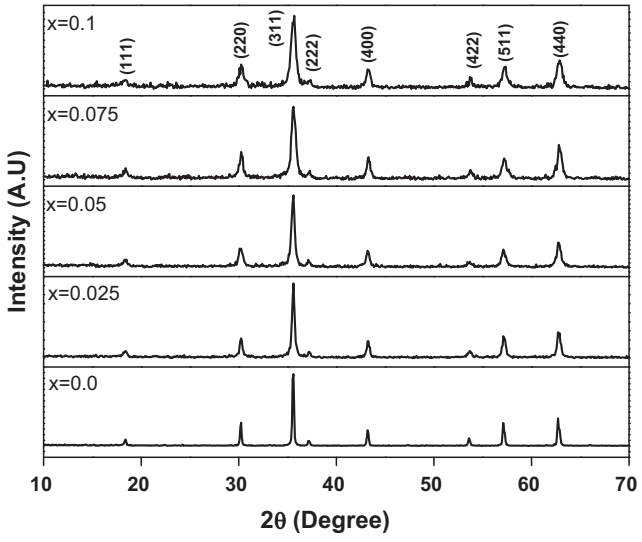

Fig. 3. XRD patterns of the sample $CoFe_{2-x}La_xO_4$ for $x = 0.0$, 0.025, 0.05, 0.075 and 0.1 annealed at 800 °C.

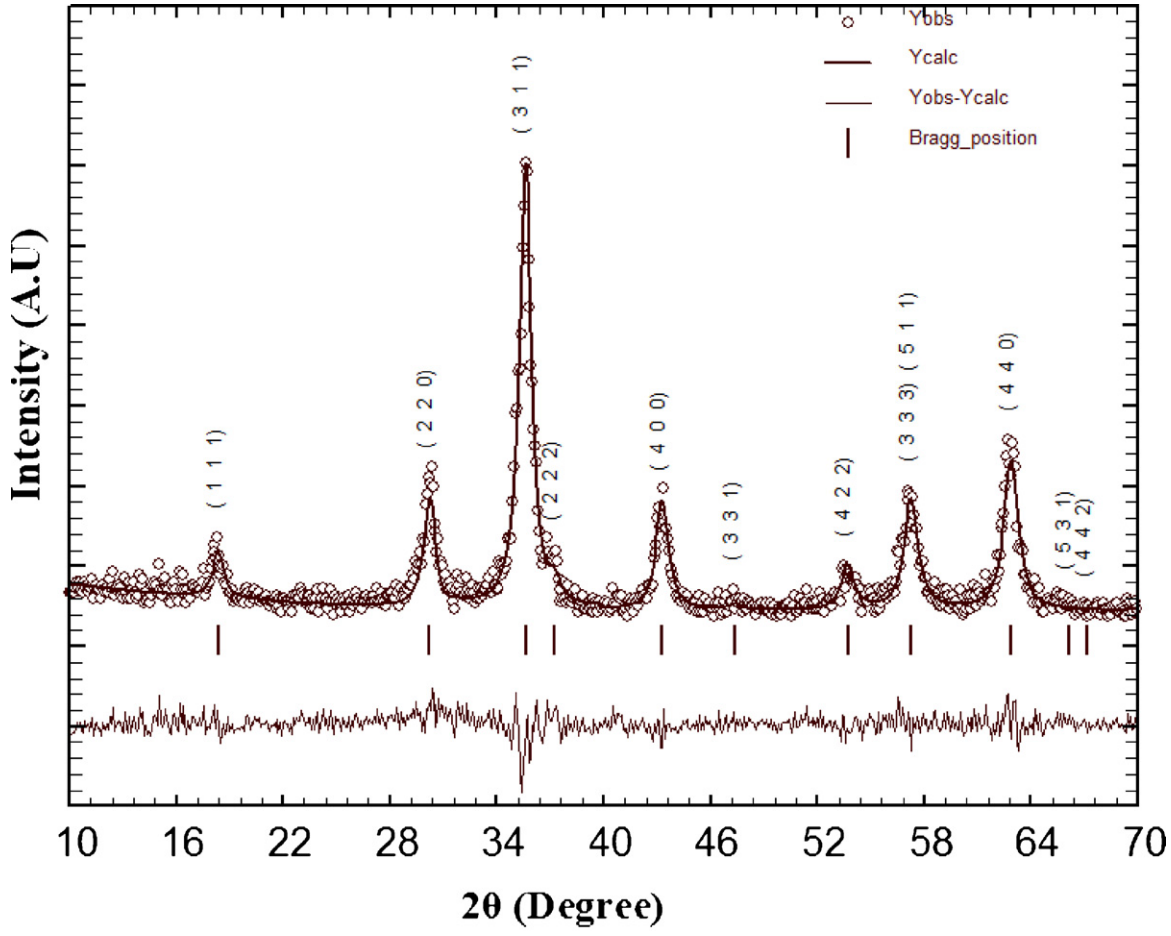

Fig. 4. Rietveld refined XRD pattern for the sample $CoFe_{1.95}La_{0.05}O_4$ annealed at 600 °C. The circles represent experimental points and the solid line represents Rietveld refined data. The bottom line shows the difference between the experimental and refined data. The marked 2θ positions are the allowed Bragg peaks.

All XRD patterns were analyzed employing Rietveld technique [34] with the help of Fullprof Suite programme. The patterns for all the samples could be refined using the $Fd\bar{3}m$ space group. Typical XRD patterns along with Rietveld refinement are shown in Figs. 4 and 5 for the samples $CoFe_{1.95}La_{0.05}O_4$ (annealed at 600 °C) and $CoFe_{1.975}La_{0.025}O_4$ (annealed at 800 °C) respectively. Here the experimental data are shown as open circles and calculated intensities are shown as solid line. The bottom line represents the difference between measured and calculated intensities. The allowed Braggs positions for the $Fd\bar{3}m$ space group are marked as vertical lines. All the observed peaks in the XRD patterns are allowed Bragg 2θ positions. The oxygen positions ($x = y = z$) were taken as free parameters and, all other atomic fractional positions were taken as fixed. Other parameters such as lattice constants, isothermal parameters, occupancies, scale factors and shape parameters were taken as free parameters. Background was refined by using pseudo voigt function.

The refined XRD patterns for all the samples annealed at 600 °C show slight deviation between observed and calculated patterns. Diffuse scattering in the diffraction pattern of nanocrystalline materials is dominant than in those of bulk crystalline materials due to large ratio of surface to volume atoms. The diffuse scattering becomes significant at the nanoscale while Bragg scattering gets diminished which leads to decrease in intensity and broadening of peaks of XRD patterns [35]. Hence the deviation is observed between experimental and calculated data for 600 °C annealed samples. However, no deviation is observed between experimental and calculated pattern for 800 °C annealed samples due to dominance of Bragg scattering. R_p is a profile factor and it is defined as,

$$R_p = 100\frac{\sum_{i=1,n}|y_i - y_{c,i}|}{\sum_{i=1,n}y_i} \quad (1)$$

where y_i is the observed point (experimental) and $y_{c,i}$ is the calculated point and n represents the number of data points. R_{wp} is a weighted profile factor which is defined as,

$$R_{wp} = 100\left[\frac{\sum_{i=1,n}\omega_i|y_i - y_{c,i}|^2}{\sum_{i=1,n}\omega_i y_i^2}\right]^{1/2} \quad (2)$$

where $\omega_i = 1/\sigma_i^2$ σ_i^2 is the variance of observation y_i. Bragg factor R_{Bragg} is defined as,

$$R_B = 100\frac{\sum_h|I_{obs,h} - I_{calc,h}|}{\sum_h I_{obs,h}} \quad (3)$$

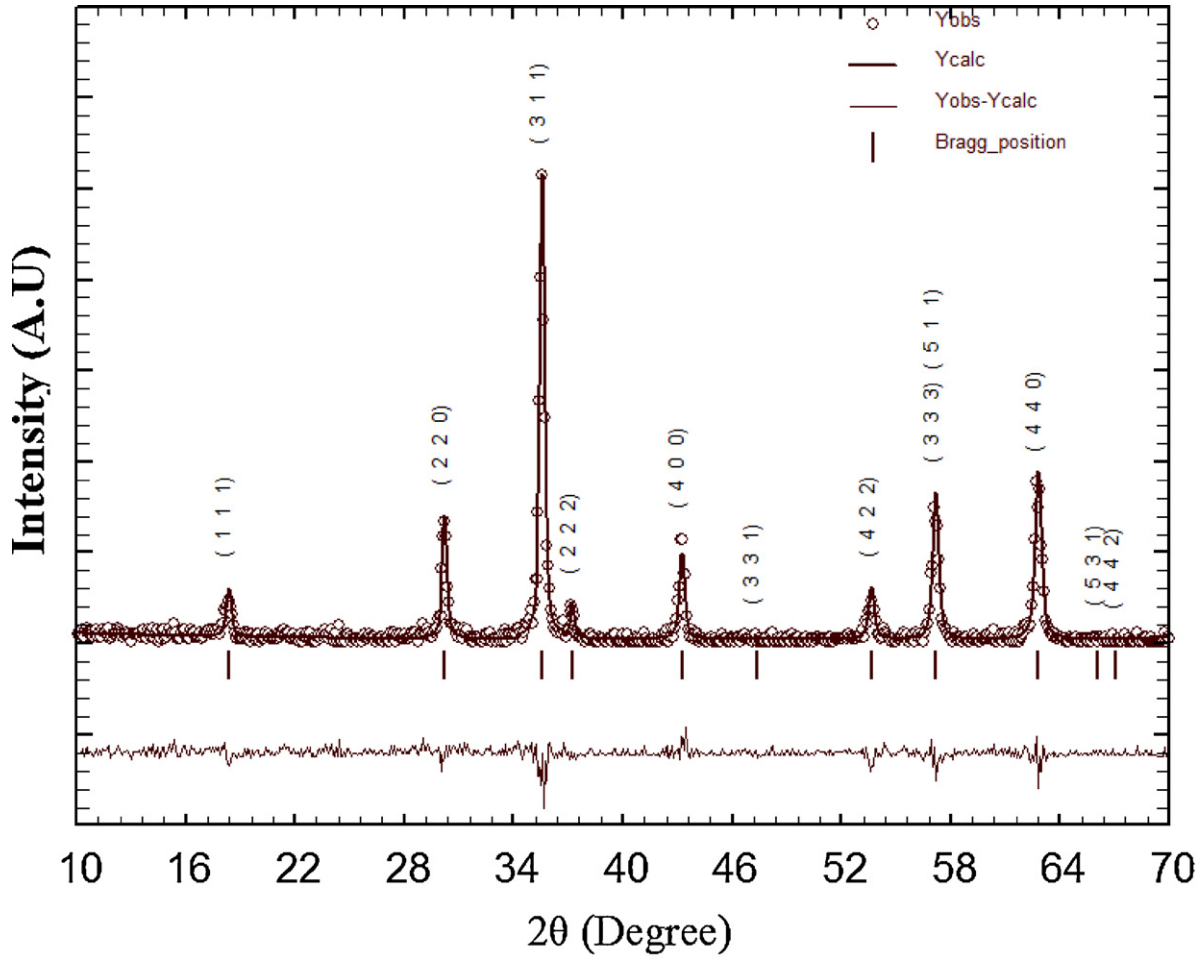

Fig. 5. Rietveld refined XRD pattern for the sample $CoFe_{1.975}La_{0.025}O_4$ annealed at 800 °C. The circles represent experimental points and the solid line represents Rietveld refined data. The bottom line shows the difference between the experimental and refined data. The marked 2θ positions are the allowed Bragg peaks.

Here 'h' is the vector which levels the Bragg reflections. The $I_{obs,h}$ is the observed integrated intensities and $I_{calc,h}$ is the calculated intensities. Crystallographic R_F factor is defined as,

$$R_F = 100\frac{\sum_h |F_{obs,h} - F_{calc,h}|}{\sum_h F_{obs,h}} \quad (4)$$

where $F_{obs,h}$ and $F_{calc,h}$ are the observed and calculated structural factors respectively. Goodness of fit is defined as,

$$\chi^2 = \left[\frac{R_{wp}}{R_{\exp}}\right]^2 \quad (5)$$

The R_p, R_{wp}, R_{Bragg}, R_F (profile factor) and χ^2 for all the samples annealed at 800 °C are listed in Table 1. The R_p and R_{wp} factors are found to be large. A similar R_p and R_{wp} factors have been observed by the other research group for nanocrystalline samples [36]. It could be due to the low signal to noise ratio of XRD patterns for nanocrystalline materials. However, we have observed a low values of χ^2 (goodness of fit), R_{Bragg} and R_F which justifies the goodness of refinement.

The analysis of the crystallite size has been carried out using the peak broadening of the XRD patterns. Peak broadening comes from several sources such as instrumental effect, finite crystallite size and strain effect within the crystallite lattice. The crystallite size of the samples have been obtained using Rietveld method, because in this method all the instrumental factors are taken into account for corrections of the peak broadening. A complete expression used in Rietveld method [34] is defined as,

$$FWHM^2 = (U + D_{ST}^2)(\tan^2\theta) + V(\tan\theta) + W + \frac{IG}{\cos^2\theta} \quad (6)$$

where U, V and W are the usual peak shape parameters, IG is a measure of the isotropic size effect, D_{ST} is the coefficient related to strain. The values of the crystallite size for the samples annealed at 200 °C, 600 °C and 800 °C are listed in

Table 1
Rietveld agreement factors for the samples $CoFe_{2-x}La_xO_4$ (x = 0.0, 0.025, 0.05, 0.075 and 0.1) annealed at 800 °C. R_p is a profile factor, R_{wp} is a weighted profile factor, R_{Bragg} is Bragg factor, R_F is Crystallographic factor and χ^2 is Goodness of fit.

	x = 0.0	x = 0.025	x = 0.05	x = 0.075	x = 0.1
R_p (%)	16.0	19.2	21.6	22.7	22.4
R_{wp} (%)	18.9	20.1	19.8	20.2	19.7
R_{Bragg}	5.2	7.9	7.5	6.1	6.9
R_F	4.1	7.1	7.8	5.0	6.2
χ^2	1.08	1.07	1.08	1.08	1.06

Table 2
Lattice constant and crystallite size for the samples $CoFe_{2-x}La_xO_4$ ($x = 0.0$, 0.025, 0.05, 0.075 and 0.1) annealed at 200 °C, 600 °C and 800 °C. ($a = b = c$ = lattice constant and D = average crystallite size). Errors in lattice parameters are given as bracket.

Samples	Annealing temperature (°C)					
	200 °C		600 °C		800 °C	
	$a = b = c$ (Å)	D (nm)	$a = b = c$ (Å)	D (nm)	$a = b = c$ (Å)	D (nm)
0.0	8.360 (67)	6.89	8.378 (22)	35.62	8.379 (27)	48.02
0.025	8.359 (36)	7.02	8.370 (31)	11.58	8.373 (53)	27.01
0.050	8.361 (27)	7.98	8.369 (43)	10.91	8.370(57)	22.11
0.075	8.359 (42)	8.08	8.371 (36)	11.02	8.365 (64)	17.05
0.1	8.358(38)	7.92	8.369 (41)	10.87	8.358 (45)	15.12

Table 2. The sizes of the crystallite have been increased with the annealing temperature. During the thermal annealing solid–vapor surface of the crystals is replaced by solid–solid interface via diffusion to reduce the overall surface energy which leads to the expansion of volume and, as an effect increase the crystallite size. We have observed that the size of the crystallite remains unchanged for $x \geq 0.025$ samples annealed at 200 °C and 600 °C even the samples were prepared in similar condition. It reveals that surface strain is dominating and thermal energy is not sufficient for the removal of strain due to the size mismatch between La^{3+} and Fe^{3+} ions. The crystallite size decreases with the increase in La concentration for the samples annealed at 800 °C. It reveals that substitution of La^{3+} ion in place of Fe ion induces a crystalline anisotropy due to large size mismatch of La^{3+} and Fe^{3+} and, this crystalline anisotropy creates strain inside the volume of crystal which increases with the increase in La^{3+} concentration. Therefore the present system remains in stable equilibrium by balancing crystal anisotropy and volume strain to each other. Hence, in order to relax the volume strain the crystallite size decreases with the increase in La^{3+} concentration.

The values of lattice constants for all the samples annealed at 200 °C, 600 °C and 800 °C are listed in Table 2. There are high errors for lattice constants (Table 2) calculation by the Rietveld analysis as samples are in nanocrystalline form. Hence we have shown a typical zoom of (3 1 1) XRD peak in Fig. 6 for the sample $x = 0.025$ annealed at 200, 600 and 800 °C. According to Bragg's law of X-ray diffraction the lattice constant for cubic structure is defined as,

$$a = \frac{\lambda(h^2 + k^2 + l^2)^{1/2}}{2\sin\theta} \tag{7}$$

Here a is the lattice constant and θ is the glancing angle. The lattice constant increases with the decrease in diffraction peak position for a particular ($h\,k\,l$) value. However, we have not observed shift of the (3 1 1) peak position (Fig. 6) with the annealing temperature. Hence, we have observed that lattice constants are almost same within the error bar of Rietveld analysis. The higher error bars are due to the nanocrystalline form of the sample. Generally, lattice constant decreases with the increase in crystallite size as the lattices go to minimum energy with the increase in size. Hence, it is required to carry out more experiments (neutron diffraction or Synchrotron radiation diffraction) to conclude the above observation which is beyond the scope of the present paper.

Lattice constants for the samples annealed at 200 °C and 600 °C are independent of La^{3+} concentration. It appears that, atoms at the surface are trapped in thermodynamically non-equilibrium states for 200 °C and 600 °C annealed samples due to surface strain. Also it is well known that, surface to volume ratio is more effective to control the crystal structure and physical properties for very low dimensional particles (in nanocrystalline order) than the symmetry of the crystal structure. The values of lattice constants for the samples annealed at 800 °C decreases with the increase in La^{3+} concentration. Similar decrease in lattice parameters have been observed for RE^{3+} (RE = rare earth cations) ions substituted nanocrystalline cobalt ferrite [37,38]. Although there are high errors in the lattice constant, we have observed the peaks shift in the XRD pattern (figure not shown). The observed decrease of lattice constant could be explained on the basis of rearrangement of cations between the A-site and B-site in order to relax the lattice strain (discussed in the next section).

Cation distributions among the tetrahedral and octahedral interstitial sites were estimated by the Rietveld refinement of occupancies. The estimated cation distributions from Rietveld analysis for the samples annealed at 600 °C and 800 °C are shown in Table 3. One can observe that the concentration of

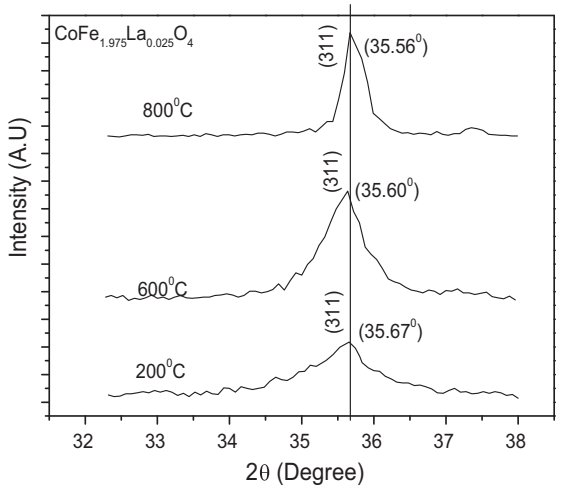

Fig. 6. Typical zoom XRD plot for $x = 0.025$ sample corresponding to peak (3 1 1) annealed at 200 °C, 600 °C and 800 °C.

Table 3
Site occupancy of cations for the samples $CoFe_{2-x}La_xO_4$ ($x = 0.0$, 0.025, 0.05, 0.075 and 0.1) annealed at 600 °C and 800 °C. Errors in occupancies are given in bracket (example: 0.110 (2) = 0.110 ± 0.002).

Samples	600 °C		800 °C	
	A-site	B-site	A-site	B-site
$x = 0.00$	$Co_{0.110(2)}Fe_{0.890(3)}$	$Co_{0.890(3)}Fe_{1.110(3)}$	$Co_{0.030(2)}Fe_{0.970(3)}$	$Co_{0.970(2)}Fe_{1.030(1)}$
$x = 0.025$	$Co_{0.275(4)}Fe_{0.724(2)}La_{0.001(2)}$	$Co_{0.725(4)}Fe_{1.251(2)}La_{0.024(3)}$	$Co_{0.108(2)}Fe_{0.890(3)}La_{0.002(3)}$	$Co_{0.892(5)}Fe_{1.085(3)}La_{0.023(3)}$
$x = 0.05$	$Co_{0.291(2)}Fe_{0.708(3)}La_{0.001(2)}$	$Co_{0.709(2)}Fe_{1.242(3)}La_{0.049(1)}$	$Co_{0.179(4)}Fe_{0.818(3)}La_{0.003(2)}$	$Co_{0.821(4)}Fe_{1.132(3)}La_{0.047(3)}$
$x = 0.075$	$Co_{0.329(2)}Fe_{0.669(2)}La_{0.002(2)}$	$Co_{0.671(3)}Fe_{1.256(3)}La_{0.073(2)}$	$Co_{0.217(2)}Fe_{0.782(4)}La_{0.001(2)}$	$Co_{0.783(3)}Fe_{1.143(4)}La_{0.074(2)}$
$x = 0.1$	$Co_{0.348(2)}Fe_{0.651(4)}La_{0.001(2)}$	$Co_{0.652(3)}Fe_{1.249(4)}La_{0.099(3)}$	$Co_{0.268(2)}Fe_{0.730(3)}La_{0.002(2)}$	$Co_{0.732(4)}Fe_{1.170(3)}La_{0.098(2)}$

La^{3+} ion is very less in the A site (within the limit of error). Hence, we conclude that the La^{3+} ions show a preference for octahedral sites. From occupancy variation we have observed that Co ion occupy both tetrahedral and octahedral sites. Hence, the present samples are in mixed spinel structure. Radius of the octahedral site is larger than the tetrahedral site in the spinel lattice. The ionic radius of the La^{3+} ion is large enough for octahedral site. One can assume that small amount of La^{3+} cations can be substituted for Fe^{3+} cations which enter into the octahedral sites by rearrangement of cations between the tetrahedral and octahedral sites to minimize the free energy of the system. Partial migration of Co^{2+} ions (0.74 Å) from B to A sites has been observed by increasing the La concentration accompanied by an opposite transfer of equivalent number of Fe^{3+} ions (0.64 Å) from A to B sites in order to relax the strain at the octahedral sites. Hence the lattice constants decrease with the increase in La concentration. Also it affects the saturation magnetization and magnetocrystalline anisotropy constant (discussed in the next section).

3.2. FT-IR analysis

The FT-IR spectroscopy is very useful technique to understand the molecular dynamics. The FT-IR absorption bands of crystalline solid are usually assigned to the vibration of ions in crystal lattices. The formation of the spinel structure in the nanocrystalline form and its cations distribution is supported by the FT-IR analysis. The FT-IR spectra of the samples annealed at 800 °C with $x = 0.0$, 0.025, 0.075 and 0.1 compositions are shown in Fig. 7. The spectra indicate the presence of absorption bands in the range of 390–750 cm^{-1} which is common feature of the spinel ferrite [39]. The higher frequency absorption band (ν_1) lies in the range 500–600 cm^{-1} and it is assigned to vibration of the tetrahedral metal complex which is the bond between the oxygen ion and the tetrahedral site metal ion (M_{Tet}–O). Lower frequency absorption band (ν_2) lies in the range of 400–490 cm^{-1} and it is assigned to vibration of the octahedral metal complex which is the bond between the oxygen ion and the octahedral site metal ion (M_{Oct}–O) [40]. These band positions are found to be in agreement with the characteristic infrared absorption bands of cobalt ferrite nanocrystals [41]. The peak position of the absorption bands changes with the doping of La ions in the place of Fe ions. The change in the band positions is due to the change in M_{Tet}–O and M_{Oct}–O bond lengths [42].

3.3. Elemental analysis

FE-SEM images of the sample $CoFe_2O_4$ ($x = 0.0$) annealed at 600 °C and 800 °C are shown in Fig. 8(a) and (b). Sizes of the particles are almost uniform. The average particle size for the sample $x = 0.0$ annealed at 600 °C is found to be 32 nm which are close to crystallite size obtained by XRD analysis (35 nm). The average particle size for sample ($x = 0.0$) annealed at 800 °C is around 0.12 μm which is larger than the crystallite size obtained from XRD (48 nm). The average particle size increases with the increase of annealing temperature. Particles have a large surface area in nanocrystalline form which suggests that several neighboring particles fuse together to agglomerate by the melting of their surface and gets bigger with increase in annealing temperature. The FE-SEM image for the sample $x = 0.1$ annealed at 800 °C (Fig. 8(c)) shows the average particle size is around 15 nm which supports that particle size decreases with the increase of La^{3+} concentration. From the above discussion it is clear that, the particle size and crystallite size are equal when the samples are in single domain region (<100 nm). However it may or may not be different for the particle above than single domain region (>100 nm). The typical EDS pattern of sample $CoFe_{1.9}La_{0.1}O_4$ annealed at 800 °C is shown in Fig. 9. The EDS spectrum reveals the presence of Co, Fe, La, Au and O elements in the sample. One can see that except the extra Au peak, there are no any other peaks appeared. The gold peak is due to the thin coating of gold on the sample surface to make it conducting. It reveals that there is no contamination in the sample.

3.4. Magnetic studies

Magnetic hysteresis loops for $CoFe_{2-x}La_xO_4$ samples annealed at 600 °C and 800 °C are shown in Figs. 10 and 11 respectively. Saturation magnetizations for the samples annealed at 600 °C and 800 °C were obtained from fitting to equation "Law of Approach to Saturation" (discussed in the next section). The values of saturation magnetization for all the samples annealed at 600 °C and 800 °C are listed in Table 4. The saturation magnetization for the samples $CoFe_{2-x}La_xO_4$ ($x = 0.0$–0.1) increases with the crystallite size. This increase in saturation magnetization is due to the increase of the crystallite size and minimization of the surface effect. We observed that (Table 4), the saturation magnetization for undoped sample annealed at 600 °C is very high compared to La doped sample.

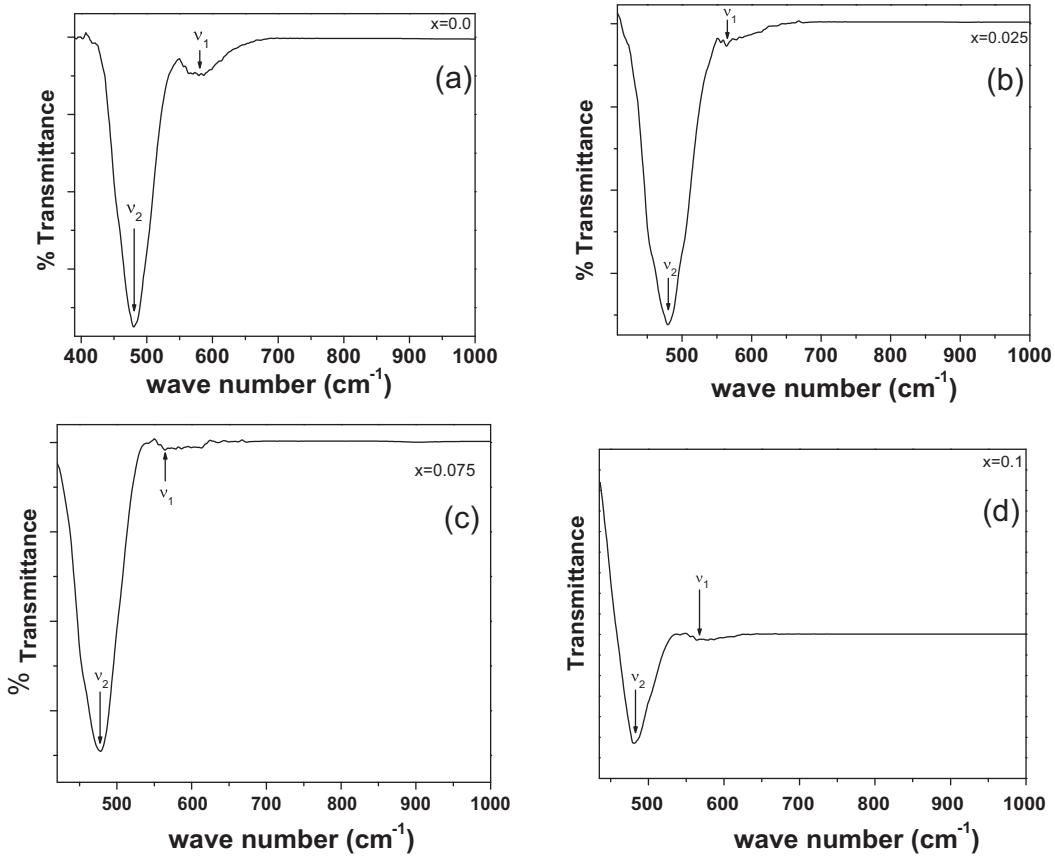

Fig. 7. The FT-IR spectra of the sample $CoFe_{2-x}La_xO_4$ with (a) $x = 0.0$, (b) $x = 0.025$, (c) $x = 0.075$ and (d) $x = 0.1$ annealed at 800 °C.

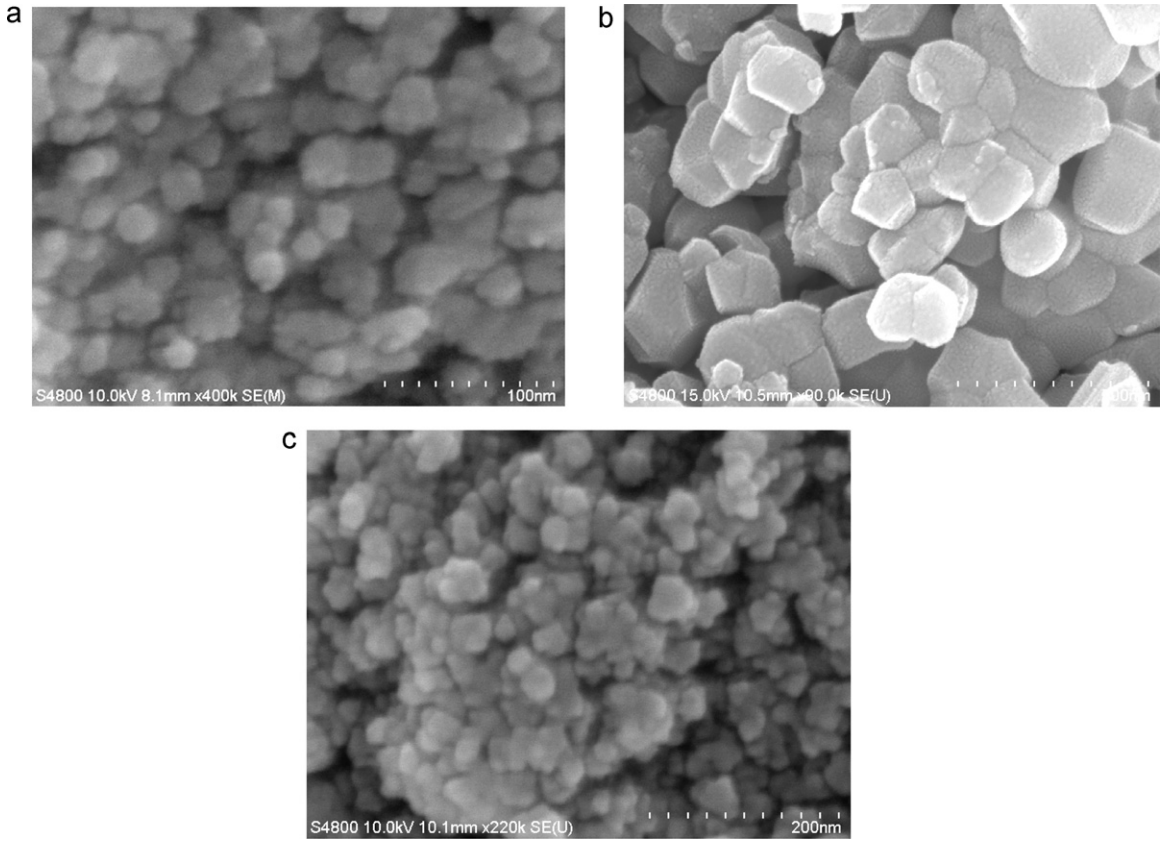

Fig. 8. FE-SEM image of the sample (a) $x = 0.0$ annealed at 600 °C (b) $x = 0.0$ annealed at 800 °C and (c) $x = 0.1$ annealed at 800 °C.

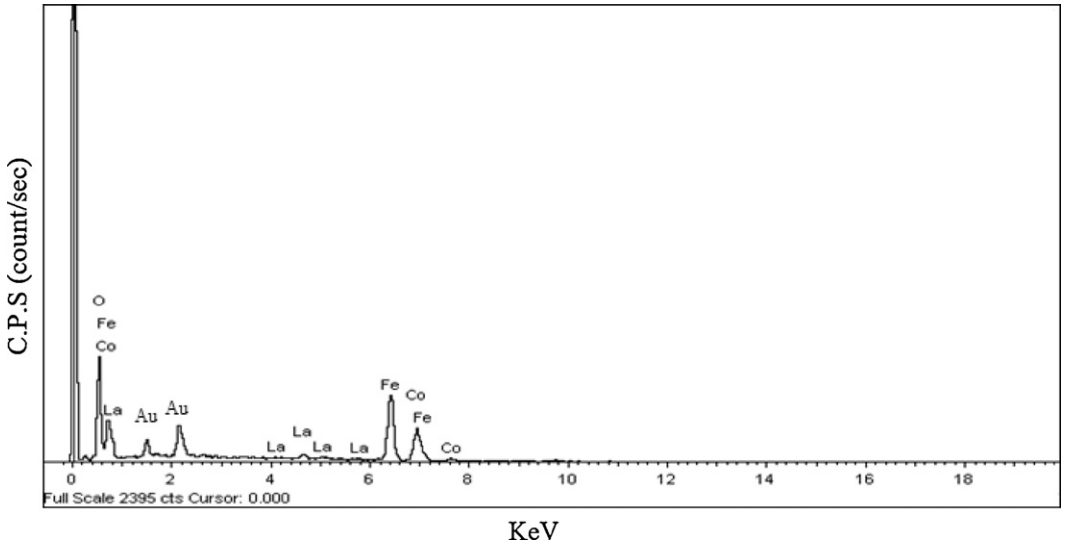

Fig. 9. The EDS pattern of sample $CoFe_{1.9}La_{0.1}O_4$ annealed at 800 °C. Au peaks are appearing due to the coating on the sample.

There is much larger lattice distortion (smaller crystallite size) at the surface which leads to a greater degree of spin disorderness. The saturation magnetization for the samples $x \geq 0.025$ annealed at 600 °C is independent of the La concentration. However, the saturation magnetization for samples annealed at 800 °C decreases with the La^{3+} concentration. The observed behavior could be attributed to two factors: (1) we have observed that crystallite size decreases with the La^{3+} concentration for the well crystallized samples. As the crystallite size decreases, the ratio of surface to volume atom increases as a result the surface effect becomes prominent. Structure is distorted at the surface and surface atoms are under the effect of strain which leads to vacancies, variety of interatomic spacing and low coordination numbers. All of these factors may induce a broken exchange bonds for the surface atoms which leads to spin disorder [43]. The disordered spin at the surface may exhibit low magnetization. Disordered spins increase with the decrease in crystallite size which leads to reduction in saturation magnetization. (2) In spinel ferrite the saturation magnetization is dominated by the superexchange interactions between the tetrahedral (A-sites) and octahedral (B-sites) sites cations. La^{3+} ions do not take part in the exchange interactions to the nearest neighboring ions as they are non magnetic (zero magnetic moment). Hence it will decrease the number of magnetic linkages occurring between tetrahedral and octahedral cations. It leads to weakening of the tetrahedral–octahedral superexchange interactions with the increase in La^{3+} concentration [44].

The values of coercivity for the samples annealed at different temperatures are listed in Table 4. The coercivity for undoped sample ($CoFe_2O_4$) decreases with the increase of annealing temperature. It could be due to the presence of magnetic multi domain in the sample annealed at 800 °C. In the multi domain

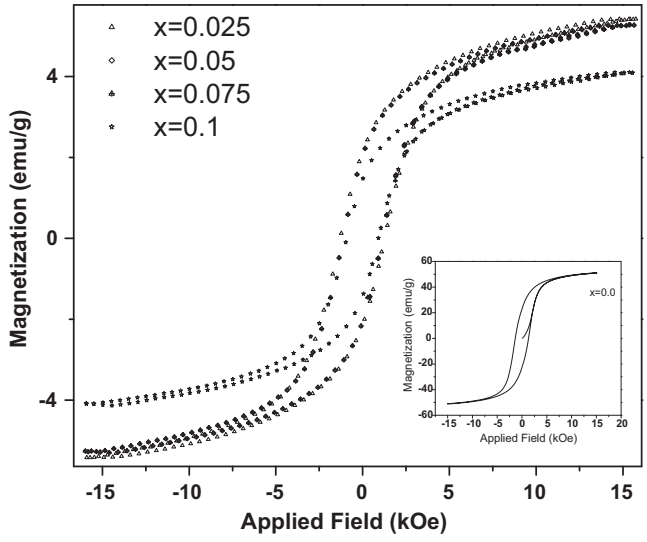

Fig. 10. Hysteresis loops for $CoFe_{2-x}La_xO_4$ ($x = 0.0$, 0.025, 0.05, 0.075 and 0.1) samples annealed at 600 °C. Insets shows the magnified hysteresis loops for the samples $x = 0.025$–0.1.

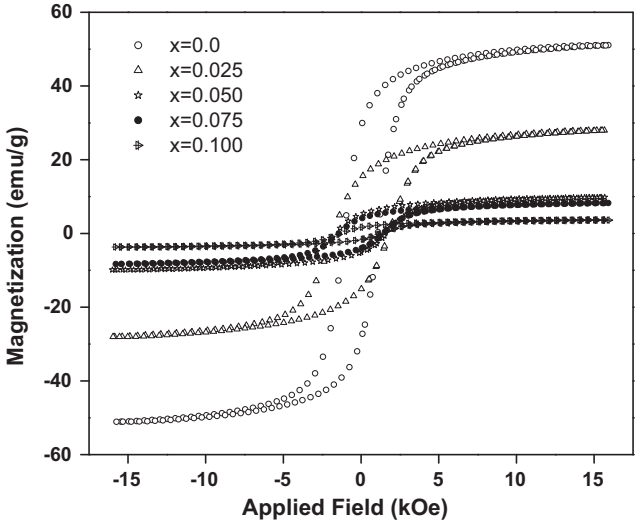

Fig. 11. Hysteresis loops for $CoFe_{2-x}La_xO_4$ ($x = 0.0$, 0.025, 0.05, 0.075 and 0.1) samples annealed at 800 °C.

Table 4
Parameters obtained from magnetic hysteresis measurement at room temperature of the samples $CoFe_{2-x}La_xO_4$ ($x = 0.0, 0.025, 0.05, 0.075, 0.1$) annealed at 600 °C and 800 °C (M_s = saturation magnetization, H_c = coercivity, K_1 = magnetocrystalline anisotropy constant).

	Annealing temperature (°C)					
	600 °C			800 °C		
	M_s (emu/g)	H_c (kOe)	K_1 (erg/cm^3)	M_s (emu/g)	H_c (kOe)	K_1 (erg/cm^3)
$x = 0.0$	49.01	1.394	2.21×10^6	52.18	1.125	2.41×10^6
$x = 0.025$	5.53	1.272	0.14×10^6	29.09	1.750	1.76×10^6
$x = 0.05$	5.32	1.137	0.13×10^6	10.29	1.625	0.87×10^6
$x = 0.075$	5.10	0.945	0.12×10^6	8.67	1.448	0.57×10^6
$x = 0.1$	4.00	0.913	0.09×10^6	3.80	1.317	0.24×10^6

region the variation of coercivity with the crystallite size can be expressed as [21],

$$H_C = e + \frac{f}{D} \tag{8}$$

where 'e' and 'f' are constants and 'D' is the crystallite size. Hence in the multi domain region the coercivity decreases as the crystallite size increases. So, we conclude that sample $CoFe_2O_4$ annealed at 800 °C is in multi domain whereas, sample annealed at 600 °C is in single domain which have been observed from the FE-SEM images.

Coercivity decreases with the increase in La concentration (crystallite size decrease with the increase of La^{3+} concentration) for the samples annealed at particular temperature (either 600 °C or 800 °C). However, we have observed that coercivity increases with the increase of annealing temperature, i.e. increase of crystallite size. In a single domain region the variation of coercivity with the crystallite size is expressed as [21],

$$H_C = g - \frac{h}{D^2} \tag{9}$$

where g and h are constant. Coercivity decreases with the decrease in crystallite size in the single domain region because of thermal effects. Hence, it appears that the crystallite sizes of the La^{3+} substituted samples are within the range of single domain size limit even after annealing at 800 °C.

Saturation magnetization data have been analyzed by the ''Law of Approach (LA)'' to saturation. The magnetocrystalline anisotropy constants of the samples $CoFe_{2-x}La_xO_4$ annealed at 600 °C and 800 °C have been calculated from the LA analysis. LA describes the dependence of magnetization M on the applied magnetic field for $H \gg H_c$. The magnetization near the saturation M_s can be written as [45],

$$M = M_S\left[1 - \frac{b}{H^2}\right] \tag{10}$$

Here $b = 8/105 \times K_1^2/\mu_O^2 M_S^2$, M is the magnetization, H is the applied magnetic field, M_s is the saturation magnetization, μ_o is the permeability of the free space, K_1 is the cubic anisotropy constant. The numerical coefficient 8/105 applies to cubic anisotropy of random polycrystalline samples. Therefore M_s and K_1 are the only fitting parameters in Eq. (5). Experimental data [M-H curve] at high field (>1 T) are fitted to Eq. (4) for the present series. Typical fitting curve to LA is shown in Fig. 12 for the sample $CoFe_{1.95}La_{0.05}O_4$ annealed at 800 °C. The values of M_s and b are obtained from fitting and, magnetocrystalline anisotropy constant (K_1) was calculated using the equation,

$$K_1 = \mu_0 M_S \sqrt{\frac{105b}{8}} \tag{11}$$

The magnetocrystalline anisotropy constants for the samples annealed at 600 °C and 800 °C are listed in Table 4. Our result for undoped sample ($CoFe_2O_4$) is comparable to the earlier reports on nanocrystalline cobalt ferrites [8]. We observed that the values of magnetocrystalline anisotropy constants (K_1) for the samples $CoFe_{2-x}La_xO_4$ increase with the annealing temperature. The magnetocrystalline anisotropy constant (K_1) of the nanoparticles depend on the crystallite size [46]. It (K_1) increases with the annealing temperature (as the crystallite size increase with the annealing temperature) due to minimization of the surface effect. The value of K_1 for the samples annealed at 800 °C decreases with the increase of La^{3+} concentration. Samples annealed at 800 °C are well crystalline. Therefore, one would expect a significant role of cation distribution on the value of K_1 rather than surface effects. The magnetocrystalline anisotropy of pure cobalt ferrite ($CoFe_2O_4$) is primarily due to the presence of Co^{2+} ions on the octahedral sites (B-sites) of the

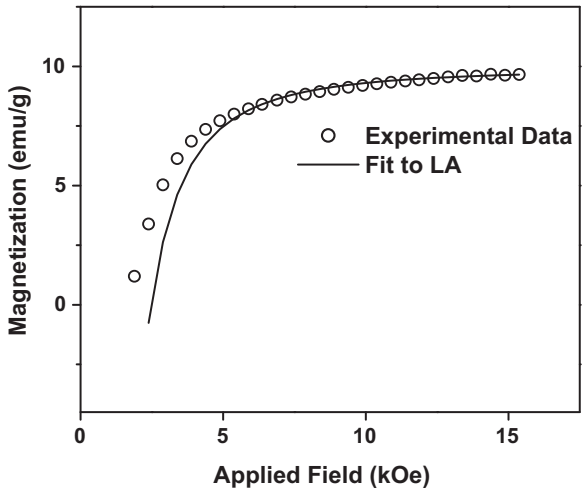

Fig. 12. Fit to LA (Law of Approach) for the samples $CoFe_{1.95}La_{0.05}O_4$ annealed at 800 °C.

spinel structure. The crystal field (trigonal field) is not capable of removing the orbital degeneracy of Co^{2+} at the octahedral sites, so that the orbital magnetic moment is not quenched and hence there is strong spin–orbit coupling (L–S coupling) which produces magnetocrystalline anisotropy energy (MAE) [21]. The values of K_1 decrease with the increase in La^{3+} concentration which is due to decrease of the occupancy of Co^{2+} ions at the B-sites (as shown in Table 4). The values of K_1 for the samples $x \geq 0.025$ annealed at 600 °C decreases marginally with the increase in La^{3+} concentration. It reveals that surface effects play a dominant role rather than cations distribution for the determination of magnetic anisotropy as the samples annealed at 600 °C are in single domain region. Generally, origin of the magnetocrystalline anisotropy is the spin–orbit coupling at the crystal lattices. Surface strain is dominant at the surface of the samples, i.e. crystal lattice are not in well define order which may perturb the crystal symmetry at the surface as a result it affects the spin–orbit coupling [47].

From above discussion we conclude that magnetocrystalline anisotropy of the present samples annealed at higher temperature (800 °C) depends on the occupancy of Co^{2+} ions at the B-sites as well as surface effect, whereas, at low annealing temperature (600 °C) the surface effect dominates the cation distribution effect.

4. Conclusion

The substitution of La ions for Fe ions in cobalt ferrite causes appreciable changes in the structural and magnetic properties. The structural parameters strongly depend on the annealing temperature. The lattice constant and crystallite size are independent of the La concentration for the samples annealed at relatively low temperature. The lattice constant and crystallite size decrease with the increase in La concentration for the samples annealed at relatively high temperature. The magnetic properties are influenced by surface effect for the samples (crystallite size <15 nm) annealed at relatively low temperature. However, the magnetic properties for the samples annealed at higher temperature depend on the cation distribution between the A-sites and B-sites as well as surface effect. Magnetocrystalline anisotropy constant increases with the increase of crystallite size and, it decreases with the increase in La^{3+} concentration. Coercivity of the present sample is highly size dependent rather than La^{3+} concentration.

Acknowledgements

The authors are thankful to the Centre of Instrumentation facility (CIF), Indian Institute of Technology Guwahati and Department of Physics, Patna University for extending the VSM and XRD facilities respectively. The authors gratefully acknowledge Department of Atomic Energy, Government of India (Sanction No. 2011/20/37P/03/BRNS/0076) for the financial support.

References

[1] A. Goldman, Modern Ferrite Technology, second ed., Springer, New York, 2006.
[2] R. Valenzuela, Magnetic Ceramics, Cambridge University Press, 1994.
[3] K. Haneda, A.H. Morrish, Non collinear magnetic structure of $CoFe_2O_4$, J. Appl. Phys. 63 (1988) 4258–4263.
[4] J. Smit, Ferrites, Wiley, New York, 1959.
[5] T. Hyeon, Chemical synthesis of magnetic nanoparticle, Chem. Commun. 8 (2003) 927–932.
[6] M. Walker, P.I. Mayo, K. O'Grady, S.W. Charles, R.W. Chantrell, The magnetic properties of single-domain particles with cubic anisotropy. I. hysteresis loops, J. Phys. Condens. Matter 5 (1993) 2779–2783.
[7] L. Kumar, M. Kar, Effect of annealing temperature and preparation condition on magnetic anisotropy in nanocrystalline cobalt ferrite, IEEE Trans. Magn. 47 (2011) 3645–3648.
[8] A. Franco Jr., F.C. e silva, High temperature magnetic properties of cobalt ferrite nanoparticles, Appl. Phys. Lett. 96 (2010) 172505–172508.
[9] E.C. Snelling, Soft Ferrites: Properties and Applications, second ed., Butterworths, London, UK, 1988.
[10] J.L. Dormann, D. Fiorani, Magnetic Properties of Fine Particles, North-Holland, Amsterdam, 1992.
[11] U. Hafeli, W. Schuut, J. Teller, M. Zborowski, Scientific and Clinical Applications of Magnetic Carriers, Plenum Press, New York, 1997.
[12] B. Zhou, Y. Zheng, C. Liao, F. Cheng, C. Yan, L. Yao, S.Y. Wang, Enhanced magneto-optical Kerr effects and decreased curie temperature in Co-Mn ferrite thin films, Appl. Phys. Lett. 79 (2001) 1849–1852.
[13] Y. Melikhov, J.E. Snyder, D.C. Jiles, A.P. Ring, J.A. Paulsen, C.C.H. Lo, K.W. Dennis, Temperature dependence of magnetic anisotropy in Mn-substituted cobalt ferrite, J. Appl. Phys. 99 (2006), 08R102–08R105.
[14] N. Ranvah, Y. Melikhov, D.C. Jiles, J.E. Snyder, A.J. Moses, P.I. Williams, S.H. Song, Temperature dependence of magnetic anisotropy of Ga-substituted cobalt ferrite, J. Appl. Phys. 103 (2008), 07E506–07E509.
[15] L. Kumar, M. Kar, Influence of Al^{3+} ion concentration on the crystal structure and magnetic anisotropy of nanocrystalline spinel cobalt ferrite, J. Magn. Magn. Mater. 323 (2011) 2042–2048.
[16] L. Myrtil, Z. Kahn, John Zhang, Synthesis and magnetic properties of $CoFe_2O_4$ spinel ferrite nanoparticles doped with lanthanide ions, Appl. Phys. Lett. 78 (2001) 3651–3654.
[17] R.N. Panda, J.C. Shih, T.S. Chin, Magnetic properties of nano-crystalline Gd-or Pr-substituted $CoFe_2O_4$ synthesized by the citrate precursor technique, J. Magn. Magn. Mater. 257 (2003) 79–86.
[18] I.P. Muthuselvam, R.N. Bhowmik, Mechanical alloyed Ho^{3+} doping in $CoFe_2O_4$ spinel ferrite and understanding of magnetic monodomain, J. Magn. Magn. Mater. 322 (2010) 767–776.
[19] L.B. Tahar, L.S. Smiri, M. Artus, A.L. Joudrier, F. Herbst, M.J. Vaulay, S. Ammar, F. Fievet, Characterization and magnetic properties of Sm- and Gd-substituted $CoFe_2O_4$ nanoparticles prepared by forced hydrolysis in polyol, Mater. Res. Bull. 42 (2007) 1888–1896.
[20] L. Zhao, Y. Cui, H. Yang, L. Yu, W. Jin, S. Feng, The Magnetic Properties of $Ni_{0.7}Mn_{0.3}Gd_xFe_{2-x}O_4$ Ferrite, Mater. Lett. 60 (2006) 104–108.
[21] B.D. Culity, Introduction to Magnetic Materials, Addision-Wesely, 1972.
[22] K.K. Bharathi, K. Balamurugan, P.N. Santosh, M. Pattabiraman, G. Markandeyulu, Magnetocapacitance in Dy-doped Ni-Ferrite, Phys. Rev. B. 77 (2008) 172401–172404.
[23] K.K. Bharathi, G. Markandeyulu, Ferroelectric and ferromagnetic properties of Gd substituted Ni-Ferrite, J. Appl. Phys. 103 (2008), 07E309–07E311.
[24] K.K. Bharathi, J.A. Chelvane, G. Markandeyulu, Magnetoelectric properties of Gd and Nd-doped Nickel Ferrite, J. Magn. Magn. Mater. 321 (2009) 3677–3680.
[25] M.A. Haj, Structural characterization and magnetization of $Mg_{0.7}Zn_{0.3}Sm_xFe_{2-x}O_4$ Ferrites, J. Magn. Magn. Mater. 299 (2006) 435–439.
[26] N. Rezlescu, E. Rezlescu, C. Pasnicu, M.L. Craus, Effects of the rare-earth ions on some properties of a Nickel–Zinc ferrite, J. Phys.: Condens Matter 6 (1994) 5707–5712.

[27] E.E. Sileo, R. Rotelo, S.E. Jacobo, Nickel zinc ferrites prepared by the citrate precursor method, Physica B 320 (2002) 257–260.
[28] S.E. Jacobo, W.G. Fano, A.C. Razzitte, The effect of rare earth substitution on the magnetic properties of $Ni_{0.5}Zn_{0.5}M_xFe_{2-x}O_4$ (M: rare earth), Physica B 320 (2002) 261–263.
[29] E.E. Sileo, S.E. Jacobo, Gadolinium–nickel ferrites prepared from metal citrates precursors, Physica B 354 (2004) 241–245.
[30] W.C. Kim, S.J. Kim, J.C. Sur, C.S. Kim, Structural and magnetic properties of $CoFe_{1.9}RE_{0.1}O_4$ (RE = Y, La) prepared by a sol–gel method, J. Magn. Magn. Mater. 242 (2002) 197–200.
[31] L.B. Tahar, M. Artus, S. Ammar, L.S. Smiri, F. Herbst, M.J. Vaulay, V. Richard, J.M. Greneche, F. Villian, F. Fievet, Magnetic properties of $CoFe_{1.9}RE_{0.1}O_4$ nanoparticles (RE = La, Ce, Nd, Sm, Eu, Gd, Tb, Ho) prepared in polyol, J. Magn. Magn. Mater. 320 (2008) 3242–3250.
[32] P. Kumar, S.K. Sharma, M. Knobel, M. Singh, Effect of La^{3+} doping on the electric, dielectric and magnetic properties of cobalt ferrite processed by co-precipitation technique, J. Alloys. Compd. 508 (2010) 115–118.
[33] S. Burianova, J.P. Vejpravova, P. Holec, J. Plocek, D. Niznansky, Surface spin effect in La-doped $CoFe_2O_4$ nanoparticles prepared by microemulsion route, J. Appl. Phys. 110 (2011), 073902–073907.
[34] R.Y. Young, The Rietveld Method, third ed., Oxford University Press, 1996
[35] N.G. Jovic, A.S. Masadeh, A.S. Kremenovic, B.V. Antic, J.L. Blanusa, N.D. Cvjeticanin, G.F. Goya, M.V. Antisari, E.S. Bozin, Effect of thermal annealing on structural and magnetic properties of lithium ferrite nanoparticles, J. Phys. Chem. C 113 (2009) 20559–20567.
[36] M. Bhagwat, A.V. Ramaswamy, A.K. Tyagi, V. Ramaswamy, Rietveld refinement study of nanocrystalline copper doped zirconia, Mater. Res. Bull. 38 (2003) 1713–1724.
[37] J. Peng, M. Hojamberdiev, Y. Xu, B. Cao, J. Wang, H. Wu, ydrothermal synthesis and magnetic properties of gadolinium-doped $CoFe_2O_4$ nanoparticles, J. Magn. Magn. Mater. 323 (2011) 133–138.
[38] X. Meng, H. Li, J. Chen, L. Mei, K. Wang, X. Li, Mössbauer study of cobalt ferrite nanocrystals substituted with rare-earth Y^{3+} ions, J. Magn. Magn. Mater. 321 (2009) 1155–1158.
[39] R.D. Waldron, Infrared spectra of ferrites, Phys. Rev. 99 (1955) 1727.
[40] C.G. Ramankutty, S. Sugunam, Surface properties and catalytic activity of ferrospinels of nickel, cobalt and copper prepared by soft chemical method, Appl. Catal. A 39 (2001) 128.
[41] S. Rana, J. Philip, B. Raj, Micelle based synthesis of cobalt ferrite nanoparticles and its characterization using Fourier transform infrared transmission spectrometry and thermogravimetry, Mater. Chem. Phys. 124 (2010) 264–269.
[42] R.C. Kamble, K.M. Song, Y.S. Koo, N. Hur, Low temperature synthesis of nanocrystalline Dy^{3+} doped cobalt ferrite: structural and magnetic properties, J. Appl. Phys. 110 (2011) 053910.
[43] R.H. Kodama, A.E. Berkowitz, E.J. McNiff, S. Foner, Surface spin disorder in $NiFe_2O_4$ nanoparticles, Phys. Rev. Lett. 77 (1996) 394–397.
[44] M.A. John Jacob, Khadar, Investigation of mixed spinel structure of nanostructured nickel ferrite, J. Appl. Phys. 107 (2010) 114310–114320.
[45] S. Chikazumi, Physics of Ferromagnetism, second ed., Oxford University Press, New York, 1997.
[46] W.S. Chiu, S. Radiman, R. Abd-Shukor, M.H. Abdullah, P.S. Khiew, Tunable coercivity of $CoFe_2O_4$ nanoparticles via thermal annealing treatment, J. Alloys. Compd. 459 (2008) 291–297.
[47] R.H. Kodama, Magnetic nanoparticles, J. Magn. Magn. Mater. 200 (1999) 359–372.